Quantum transport in nonlinear Rudner-Levitov models

Lei Du,[1] Jin-Hui Wu,[2] M. Artoni,[3,*] and G. C. La Rocca[4,†]

[1] *Beijing Computational Science Research Center, Beijing 100193, China*
[2] *Center for Quantum Sciences and School of Physics, Northeast Normal University, Changchun 130024, China*
[3] *Department of Engineering and Information Technology and INO-CNR Sensor Lab, Brescia University, 25133 Brescia, Italy*
[4] *NEST, Scuola Normale Superiore, 56126 Pisa, Italy*

(Dated: September 29, 2022)

Quantum transport in a class of nonlinear extensions of the Rudner-Levitov model is numerically studied in this paper. We show that the quantization of the mean displacement, which embodies the quantum coherence and the topological characteristics of the model, is markedly modified by nonlinearities. Peculiar effects such as a "trivial-nontrivial" transition and unidirectional long-range quantum transport are observed. These phenomena can be understood on the basis of the dynamic behavior of the effective hopping terms, which are time and position dependent, containing contributions of both the linear and nonlinear couplings.

I. INTRODUCTION

The Rudner-Levitov (RL) model [1], which can be viewed as a simple non-Hermitian extension of the Su-Schrieffer-Heeger (SSH) model [2], has been predicted to support quantized quantum transport with topological protection [1, 3] has been verified experimentally in a lattice of optical waveguides [4]. This important feature not only shows the possibility of accessing nontrivial topological phases in physical systems where dissipations are intrinsic and unavoidable, but also provides a direct way to detect the topology of such systems by monitoring their bulk properties. Specifically, for a dimerized ladder of discrete quantum states, with one sublattice lossy and the other one neutral, the mean displacement of a particle which is initialized at a neutral site shows well quantized behaviors, depending on the ratio between the intra- and inter-cell coupling constants.

Recently, the intersection of nonlinear optics and topological photonics has unlocked a series of peculiar effects that have no counterparts in condensed matter topologies [5], such as magnet-free nonreciprocity [6, 7], active tunability [8–10], self-induced topological transitions [11–14], topological solitons [15–19], and topological frequency conversions [20–22]. Most recently, Xia *et al.* have considered a nonlinear PT-symmetric optical waveguide lattice to investigate the mutual interplay between topology, PT symmetry, and nonlinearity [23], demonstrating that global effects, i.e., topological and PT transitions, can be actively controlled by the local nonlinearity. The RL model has already been generalized by including on-site Kerr-type nonlinearities, which shows that the quantized quantum transport is severely affected by the nonlinearity induced decoherence effects [24] and that the nonlinear effect becomes pronounced in the PT-broken region [25]. However, the study of the influence of nonlinearity on the quantum transport in the RL model is still at the initial stage. In particular, work on how nonlinearities affect the hopping terms, rather than the on-site energies, is still missing; the latter in fact may affect quantum transport in the RL model precisely because its topological properties are dictated by the ratio between the intra- and inter-cell coupling constants.

In this paper, we consider specific extensions of the RL model with different types of nonlinear couplings and numerically study the quantum transport therein. As it happens for the case of on-site nonlinearities [24, 25], our results show that the nonlinear coupling generates departures from the typical quantized behavior of the particle transport. Our hopping nonlinearities turn out to be responsible for new effects, such as (*i.*) a "trivial-nontrivial" transition, by which the mean displacement will always take the value of 0 or 1 regardless of the linear coupling imbalance, and (*ii.*) a long-range transport, by which the particle can move unidirectionally across many unit cells before its decay. These phenomena can be understood on the basis of the dynamic behavior of the effective time and position dependent hopping terms containing contributions of both the linear and nonlinear couplings. Our findings are relevant to experimental platforms, such as arrays of coupled optical waveguides and cavities, but may also be adapted to acoustic or electric circuit resonators as well as superconducting quantum circuits [26–28].

II. THE RUDNER-LEVITOV MODEL

We start by briefly reviewing the original RL model [1, 3, 4], where each unit cell of the one-dimensional dimerized lattice contains a lossy site A and a neutral site B, as shown in Fig. 1. The intra- and inter-cell coupling constants are denoted by μ and ν, respectively, while the decay rate of each lossy site is denoted by γ_a. In the lossless limit $\gamma_a \to 0$, such a linear bipartite lattice is equivalent to the SSH model [2] which shows a topological transition depending on the ratio μ/ν [29, 30]. It

* artoni@lens.unifi.it
† larocca@sns.it

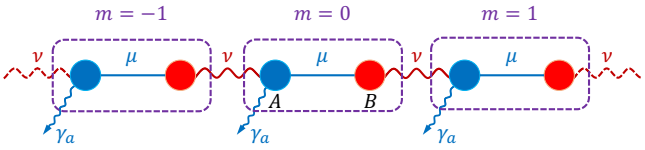

FIG. 1. (Color online) Schematic illustration of the Ruder-Levitov model, where μ (ν) and γ_a are the intracell (intercell) coupling constant and the decay rate of the lossy sites, respectively.

has been shown that the nonvanishing loss in the RL model plays the key role for observing quantized quantum transport. The real-space Hamiltonian of the RL model is given by ($\hbar = 1$ hereafter)

$$H_0 = \sum_m \Big[-i\gamma_a |m,a\rangle\langle m,a| - (\nu |m,a\rangle\langle m-1,b| + \mu |m,a\rangle\langle m,b| + \text{H.c.})\Big], \tag{1}$$

where $m \in [-N, N]$ labels the unit cells of the lattice; $|m,a\rangle$ and $|m,b\rangle$ denote the Wannier states of sites A and B in the mth unit cell, respectively.

Setting $|\psi(t)\rangle = \sum_m [a_m(t)|m,a\rangle + b_m(t)|m,b\rangle]$ as a general eigenstate of the system, with a_m (b_m) the field amplitude of A (B) in the mth unit cell, it is straightforward to attain the following dynamic equations

$$\begin{aligned} \frac{\partial a_m}{\partial t} &= -\gamma_a a_m + i\nu b_{m-1} + i\mu b_m, \\ \frac{\partial b_m}{\partial t} &= i\mu a_m + i\nu a_{m+1}. \end{aligned} \tag{2}$$

Hereafter in this paper, we assume $\mu = 0.5 - \delta g$ and $\nu = 0.5 + \delta g$ with δg denoting the coupling imbalance ($|\delta g| \le 0.5$). Then one can numerically calculate the mean displacement of a particle before its decay, i.e.,

$$\langle \Delta m \rangle = \sum_m m \int_0^\infty 2\gamma_a |a_m(t)|^2 dt. \tag{3}$$

This is equivalent to the winding number of the relative phase between components of the Bloch wave function [i.e., the eigenstate of the Fourier transformation of $H(m)$] and is thus topologically protected [1, 3, 29, 30]. Specifically, if one initializes a single particle at a neutral site, the mean displacement $\langle \Delta m \rangle$ takes the value of 0 for $\nu < \mu$ and takes the value of 1 for $\nu > \mu$, which precisely predicts the topological phase transition of this model. Note that the mean displacement always vanishes if the particle is initialized on a lossy site.

Such an archetype model has been well investigated both theoretically [1, 3] and experimentally [4], and has also been extended in many directions [24, 25, 31–39]. In the following, we generalize the RL model to a few instances with nonlinear hopping terms and study the quantum transport therein.

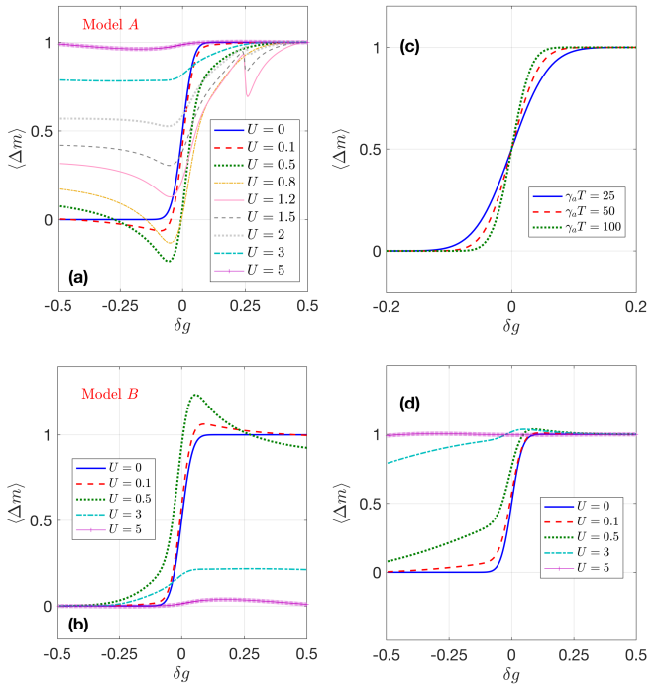

FIG. 2. (Color online) Mean displacement $\langle \Delta m \rangle$ of the particle versus coupling imbalance δg for model A [(a)] and model B [(b)], with initial state $|\psi(t=0)\rangle = |m = 0, b\rangle$, integral time $\gamma_a T = 50$, and different values of nonlinear coefficient U. (c) $\langle \Delta m \rangle$ versus δg for model A with $|\psi(t=0)\rangle = |m = 0, b\rangle$, $U = 0$, and different values of integral time T. (d) $\langle \Delta m \rangle$ versus δg for model A, with identical parameters to those in (a) except for $\mu \to -\mu$ and $\nu \to -\nu$. Other parameters are $\mu = 0.5 - \delta g$, $\nu = 0.5 + \delta g$ and$\gamma_a = 2$.

III. NONLINEARITY INDUCED TRIVIAL-NONTRIVIAL TRANSITION

We anticipate that all our nonlinear extensions have symmetric nonlinear couplings so that the norm of a quantum state still evolves according to $d\langle\psi|\psi\rangle/dt = -\sum_m 2\gamma_a |a_m|^2$ as in the linear RL model (see Appendix A); this validates in turn the definition of the mean displacement in Eq. (3). In the absence of losses, this assures the conservation of the standard norm of a quantum state; other nonlinear models, such as those related to the Ablowitz-Ladik system [40–42], do not have this property and are outside the scope of this paper. Moreover, we treat all models below as non-standard Bose-Hubbard models [41, 43], which can be well described by discrete nonlinear Schrödinger equations in the mean-field limit.

Model A. First, consider the case in which the *intercell coupling* terms contain a Kerr-type nonlinear part that depends on the field amplitudes of both lossy and neutral sites. The relevant dynamics follows the nonlinear

Schrödinger equations

$$\begin{aligned}\frac{\partial a_m}{\partial t} &= -\gamma_a a_m + i\mu b_m + i(\nu - \xi_m) b_{m-1}, \\ \frac{\partial b_m}{\partial t} &= i\mu a_m + i(\nu - \xi_{m+1}) a_{m+1}.\end{aligned} \tag{4}$$

where $\xi_m = U(|a_m|^2 + |b_{m-1}|^2)$ corresponds to the nonlinear part of the intercell coupling between the mth and $(m-1)$th unit cells, the strength of which is described by the nonlinear coefficient U. Eq. (4) embeds a non-Hermitian extension of the model in Ref. [11] and can be employed to describe arrays of coupled optical and acoustic cavities, as well as circuit resonators.

We plot in Fig. 2(a) the mean displacement $\langle \Delta m \rangle$ as a function of the coupling imbalance δg for model A with the initial state $|\psi(t=0)\rangle = |m = 0, b\rangle$. In the absence of nonlinearities ($U = 0$), the mean displacement of the particle before its decay is quantized with two integer values 0 and 1: the particle initially localized at the central neutral site will hop to the lossy site in the right ($m = 1$) unit cell and then decays from the lattice if $\nu > \mu$, or it will hop to the left lossy site within the initial ($m = 0$) unit cell and then decays if $\nu < \mu$. Note that the transition from $\langle \Delta m \rangle = 0$ to $\langle \Delta m \rangle = 1$ here is not perfectly quantized due to the finite integration time. As shown in Fig. 2(c), the quantization behavior becomes more and more ideal with the increase of the integration time T. As the nonlinear coefficient increases from zero, the mean displacement deviates from the quantized behavior gradually. In particular, the original "topological trivial" region (where $\langle \Delta m \rangle = 0$ in the linear case [1, 3]) almost disappears for upon increasing U, with the values of $\langle \Delta m \rangle$ approaching unity over the whole parametric range. In other words, the particle always hops to the right unit cell for large enough U, regardless of the relative values of μ and ν. As shown in Fig. 2(a), however, the value of $\langle \Delta m \rangle$ changes with U in a non-monotonic manner: in the nonlinear case, one can observe some dips of $\langle \Delta m \rangle$, which change non-monotonically with U and tend to vanish for strong enough nonlinearity. Clearly, the non-monotonic behavior (dip) arises at larger values of δg as U increases. We will discuss this phenomenon in detail below.

Model B. We consider next the case in which the *intracell coupling* is instead modified by a Kerr-type nonlinearity. The dynamics can now be described by,

$$\begin{aligned}\frac{\partial a_m}{\partial t} &= -\gamma_a a_m + i(\mu - \zeta_m) b_m + i\nu b_{m-1}, \\ \frac{\partial b_m}{\partial t} &= i(\mu - \zeta_m) a_m + i\nu a_{m+1},\end{aligned} \tag{5}$$

with $\zeta_m = U(|a_m|^2 + |b_m|^2)$ and the corresponding numerical results are plotted in Fig. 2(b). It can be seen that the mean displacement for model B shows exactly reverse behaviors compared with those for model A: upon increasing U, the originally "nontrivial" region (where $\langle \Delta m \rangle = 1$ in the linear case) almost disappears. In this case, the particle always hops from a neutral site to the left lossy one within the same unit cell. As a matter of fact, the results in Figs. 2(a) and 2(b) can be well understood from a sort of reflection symmetry of models A and B: the two models can be transformed into each other via $\delta g \to -\delta g$ and $\langle \Delta m \rangle \to 1 - \langle \Delta m \rangle$ [i.e., flipping the x- and y-axes simultaneously in Figs. 2(a) and 2(b)].

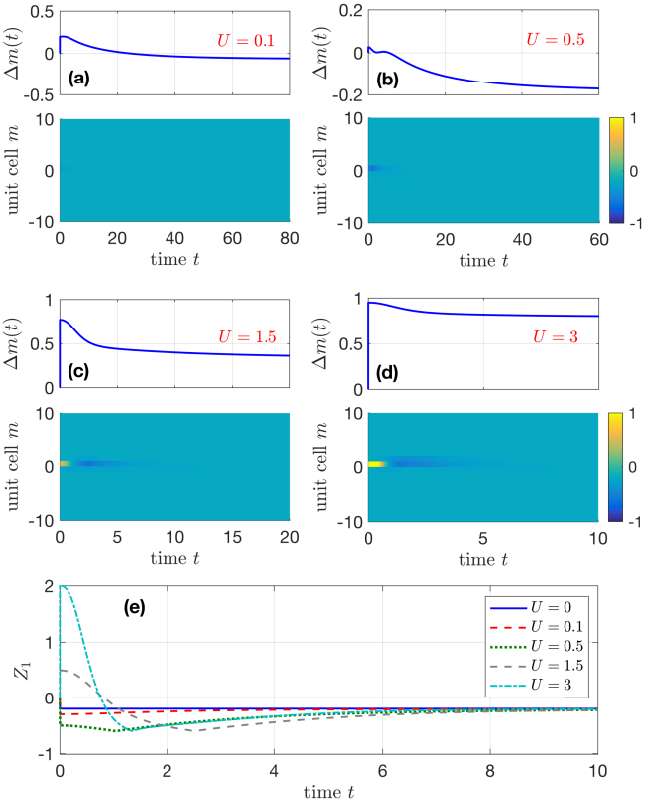

FIG. 3. (Color online) Dynamic evolutions of displacement $\Delta m(t)$ (upper) and effective coupling contrast $Z_m(t)$ (lower) for model A, with (a) $U = 0.1$, (b) $U = 0.5$, (c) $U = 1.5$, and (d) $U = 3$. (e) Dynamic evolutions of effective coupling contrast $Z_1(t)$ with different values of U. The initial state is assumed as $|\psi(t=0)\rangle = |m = 0, b\rangle$. Other parameters are $\delta g = -0.1$ and $\gamma_a = 2$.

The results above can be understood from the *effective inter- and intra-cell couplings* which contain the contributions of both the linear and nonlinear parts. As an example, we define for model A the effective coupling contrast $Z_m = |\nu_{\text{eff},m}| - |\mu|$ with $\nu_{\text{eff},m} = \nu - \xi_m$ the effective intercell coupling constant, and plot in Fig. 3 the dynamic evolutions of Z_m with different values of U. Moreover, we also plot the evolutions of the time-dependent particle displacement $\Delta m(t) = \sum_m m \int_0^t 2\gamma_a |a_m(t')|^2 dt'$ [24] showing how it reaches its final value. In the absence of nonlinearities, the coupling contrast Z_m reduces to $Z = |\nu| - |\mu|$, which is constant and can be used to predict the transition of $\langle \Delta m \rangle$, i.e., $\langle \Delta m \rangle = 1$ if $Z > 0$ and $\langle \Delta m \rangle = 0$ if $Z < 0$. In the presence of nonlinearities, however, Z_m becomes depen-

dent on m. As shown in Figs. 3(a)-3(d), the value of $Z_{m=1}$ exhibits a non-monotonic dependence on U. Such a non-monotonic behavior can be further seen in Fig. 3(e), where Z_1 first diminishes to a negative minimum before increasing with U gradually. This is coincident with the fact that the the mean displacement changes non-monotonically with U in this case. In Appendix B, we provide a detailed explanation for the physical meaning of the positive and negative fractional values of $\langle \Delta m \rangle$. As a consequence, the topology in the "trivial" region can be effectively modified by the nonlinearity and thus one can always observe nontrivial quantum transport for large enough U. In the long-time limit, the particle displacement approaches its final value and the nonlinearity induced modification vanishes. This makes sense because the influence of the nonlinear couplings fades as the particle spreads out and decays from the lattice via the lossy sites. Similarly, the "nontrivial-to-trivial" transition of model B can also be understood from the effective coupling contrast.

In Eqs. (4) and (5), we have assumed that the nonlinearities are repulsive, i.e., the signs of μ and ν are opposite to that of U. Such an assumption is responsible for the non-monotonic behavior of $\langle \Delta m \rangle$ as U changes: the non-monotonic behavior is related to a change of sign in $\nu_{\text{eff},1}$ and thus arises at larger values of δg as U increase. For comparison, we consider attractive nonlinearities by reversing the signs of sign of μ and ν (i.e., $\mu \to -\mu$ and $\nu \to -\nu$) in Eq. (4) and plot in Fig. 2(d) $\langle \Delta m \rangle$ versus δg in this case. It can be seen that the values of $\langle \Delta m \rangle$ in the originally trivial region increase monotonously with U to approach unity. This is distinct from the non-monotonic behavior in Fig. 2(a). Such a result is due to the fact that the effective coupling contrast $Z_{m=1}$ increases with U monotonously in this case.

At the end of this section, we would like to point out that the "trivial-nontrivial" transition can also be observed even if the nonlinear coupling terms only depend on the field amplitudes of the neutral sites. To prove this, we consider in Appendix C such a case and demonstrate the behaviors of the quantum transport therein.

IV. NONLINEARITY INDUCED UNIDIRECTIONAL LONG-RANGE DISPLACEMENT

Model {C. & D.} Finally, we consider in this section the case in which the nonlinear coupling constants are only dependent on the field amplitudes of the lossy sites. The relevant dynamic equations take the form (*Model C.)*,

$$\begin{aligned} \frac{\partial a_m}{\partial t} &= -\gamma_a a_m + i\mu b_m + i(\nu - \chi_m) b_{m-1}, \\ \frac{\partial b_m}{\partial t} &= i\mu a_m + i(\nu - \chi_{m+1}) a_{m+1} \end{aligned} \tag{6}$$

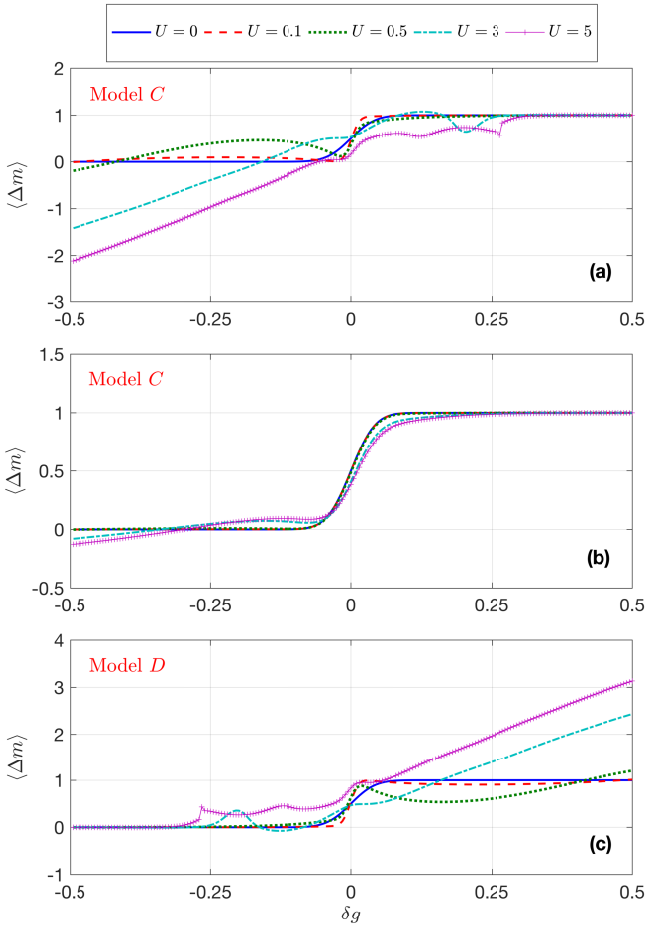

FIG. 4. (Color online) Mean displacement $\langle \Delta m \rangle$ of the particle versus coupling imbalance δg for [(a) and (b)] model C and (c) model D, with initial state $|\psi(t=0)\rangle = |m = 0, b\rangle$ and different values of nonlinear coefficient U. We assume $\gamma_a = 0.2$ for (a) and (c), while $\gamma_a = 2$ for (b).

with $\chi_m = U|a_m|^2$ describing the nonlinear part of the intercell couplings in this case. Similarly, when the intracell couplings are modified by the field amplitudes of the lossy sites in a nonlinear manner one has for the dynamic equations (*Model D.*),

$$\begin{aligned} \frac{\partial a_m}{\partial t} &= -\gamma_a a_m + i(\mu - \chi_m) b_m + i\nu b_{m-1}, \\ \frac{\partial b_m}{\partial t} &= i(\mu - \chi_m) a_m + i\nu a_{m+1}. \end{aligned} \tag{7}$$

Once again, models C and D can be transformed into each other by the reflection symmetry in the same way as models A and B can.

As in the last section, we first examine the mean displacement $\langle \Delta m \rangle$ of the particle versus the coupling imbalance δg for both models C and D, as shown in Figs. 4(a)-4(c). Interestingly, we find that long-range particle displacements, i.e., $\langle \Delta m \rangle < 0$ or $\langle \Delta m \rangle > 1$, are allowed within these two extensions of the RL model. As shown in Fig. 4(a), for instance, the value of $\langle \Delta m \rangle$ can

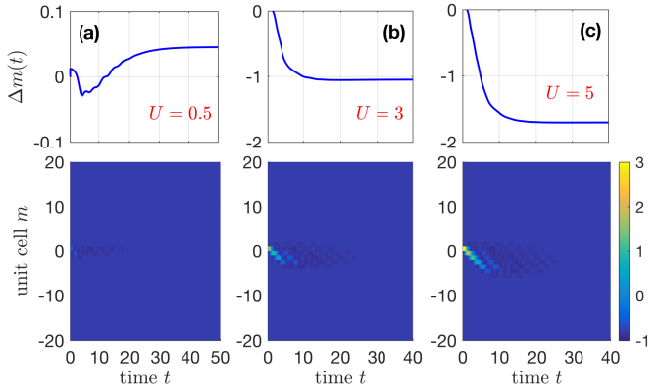

FIG. 5. (Color online) Dynamic evolutions of displacement $\Delta m(t)$ (upper) and effective coupling contrast Z_m (lower) for model C, with (a) $U = 0.5$, (b) $U = 3$, and (c) $U = 5$. The initial state is assumed as $|\psi(t = 0)\rangle = |m = 0, b\rangle$. Other parameters are $\delta g = -0.4$ and $\gamma_a = 0.2$.

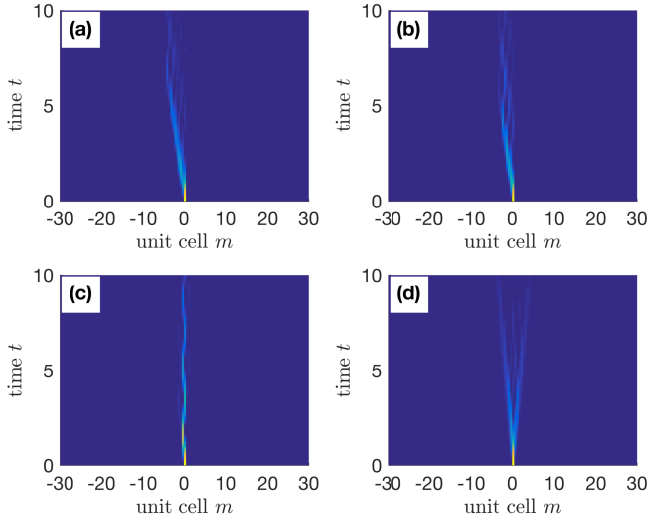

FIG. 6. (Color online) Dynamic evolutions of initial state $|\psi(t = 0)\rangle = |m = 0, b\rangle$ for model C with (a) $U = 5$ and $\delta g = -0.4$, (b) $U = 3$ and $\delta g = -0.4$, (c) $U = 0.5$ and $\delta g = -0.4$, and (d) $U = 0.5$ and $\delta g = 0$. In all cases, we take $\gamma_a = 0.2$.

be smaller than -1 for large U, implying that the particle initially located at a neutral site can hop on average several times to the left before its decay if the nonlinearities are strong enough. Note that a relatively small γ_a ($\gamma_a = 0.2$) is assumed in this case in order to observe the such unidirectional long-range displacements, while for large γ_a the mean displacement becomes less sensitive to U, as shown in Fig. 4(b). Moreover, model D displays reverse behaviors of the mean displacement, i.e., the particle will move to the right with $\langle \Delta m \rangle > 1$ for large enough U.

The underlying physics of the above results can be qualitatively understood as follows. For positive δg the intercell coupling is stronger than the intracell one, thus the particle initially localized at a neutral site will hop to the right lossy site and eventually decay. In this case, the value of the mean displacement cannot be larger than 1, because the particle will not keep on moving due to the weak intracell coupling. In contrast, for negative δg, the particle will hop to the left lossy site within the initial unit cell (i.e., the 0th unit cell in Fig. 4). For model C, the effective intercell coupling between the 0th and -1th unit cells is enhanced after the particle has moved to the site $|m = 0, a\rangle$. If the nonlinearity is strong enough, the particle can keep on moving towards the left and thereby the mean displacement should increase with U. Of course, owing to the dissipation at each lossy site, the mean displacement is still finite since the effective intercell coupling will no longer be stronger than the adjacent intracell coupling after the particle has moved across several lossy sites. This is also why the long-range particle displacement tends to vanish if the decay rate γ_a is large enough. The reverse behaviors in model D can be interpreted in a similar way.

Similar to the last section, we plot in Figs. 5(a)-5(c) the dynamic evolutions of the time-dependent displacement $\Delta m(t)$ as well as the effective coupling contrast $Z_m = |\nu - \chi_m| - |\mu|$ of model C with different values of U. Once again, one can find that the values of Z_m in a certain region increase with U. Unlikely in Fig. 3, however, where only the nearest-neighbor intercell coupling (the coupling between the 0th and the 1th unit cells) is markedly modified by the nonlinearities, here model C exhibits a larger modification region that extends toward the left side of the model. This again reflects the origin of the long-range displacements. For all cases in Fig. 5, the particle displacement reaches its final value as the modification region disappears.

The results in Fig. 5 can also be verified by the time evolutions of the initial state $|\psi(t = 0)\rangle = |m = 0, b\rangle$. As shown in Figs. 6(a)-6(c), the particle transport tends to be unidirectional as the nonlinearities strengthen. Note that for $\delta g = 0$, the lattice is homogeneous at the initial time, such that the particle transport should be almost symmetric, insensitive to the value of U. As an example, Fig. 6(d) shows the dynamic evolution of the initial state for $\delta g = 0$ and $U = 0.5$, which is similar to the symmetric diffusion in a one-dimensional homogeneous lattice. In Fig. 6(c), however, the excitation is confined within a narrow region around $m = 0$ because the effective intercell couplings are extremely weak (both the linear and nonlinear parts are weak) in this case.

V. SUMMARY AND CONCLUSIONS

In summary, we have extended the Rudner-Levitov (RL) model allowing for nonlinear hopping and assessed how nonlinearities affect the mean displacement in quantum transport. At variance with on-site nonlinearities, dynamic modifications of the ratio between the effective intra- and inter-cell couplings directly affect the behavior

of quantum transport related to the topological characteristics of the RL model. Our results encompass different extensions of the RL model, which are interpreted qualitatively in terms of the local and time-dependent effective coupling contrast function $Z_m(t)$. There is one specific extension (See Sect. IV) whereby for strong nonlinearities and low losses unidirectional long-range quantum transport may emerge.

The interplay of nonlinearity, non-Hermiticity, and topology has recently attracted much interest (see, e.g., Ref. [23]). In this paper, we introduce nonlinear deformations on a prototype model, i.e., the Rudner and Levitov non-Hermitian version of the well-known Su-Schrieffer-Heeger model. In principle, nonlinearities can be introduced either through the on-site energies or the inter-site couplings. The resulting effect, however, are non-universal, depending on either the form of the nonlinearity or the model geometry, and we considered here a few simple cases. Specifically, we carry out a detailed analysis of how the mean displacement can serve as a manifestation of the topological characteristics of the RL model even in the presence of nonlinearities. Our findings shed light on how the mean displacement is affected by the effective local dynamical environment induced by the nonlinear inter-site couplings. We would like to stress that the tight-binding Hamiltonians considered in this paper, just as the original linear ones, are general and thus have a broad relevance. Such theoretical models have indeed been extensively employed in a variety of contexts [44–46]. Our extended model is thus expected to be a good benchmark to study the interplay of nonlinearity, non-Hermiticity, and topology.

ACKNOWLEDGMENTS

This work is supported by the National Natural Science Foundation of China (No. U1930402 and No. 12074061), the Cooperative Program by the Italian Ministry of Foreign Affairs and International Cooperation (MAECI) through Italy-China International Cooperation (PGR00960), and the "Laboratori Congiunti" 2019 Program of National Research Council (CNR) of Italy.

Appendix A: Norm evolution with symmetric couplings

It has been shown that the norm of a quantum state should evolve according to

$$\frac{d}{dt}\langle\psi|\psi\rangle = -\sum_m 2\gamma_a|a_m|^2 \tag{A1}$$

to guarantee the validity of the definition of the mean displacement in Eq. (3) [1]. In this appendix, we would like to prove that Eq. (A1) still holds for nonlinear RL models with symmetric couplings. For example, according to Eq. (4) in the main text, the norm of a quantum state in model A should follows

$$\begin{aligned}
\frac{d\langle\psi|\psi\rangle}{dt} &= (\frac{d}{dt}\langle\psi|)|\psi\rangle + \langle\psi|(\frac{d}{dt}|\psi\rangle) \\
&= \sum_m \Big[(\frac{da_m^*}{dt})a_m + (\frac{db_m^*}{dt})b_m \\
&\quad + a_m^*(\frac{da_m}{dt}) + b_m^*(\frac{db_m}{dt})\Big] \\
&= \sum_m \Big[-\gamma_a|a_m|^2 - ig_r b_m^* a_m - i(g_l-\xi_m)b_{m-1}^* a_m \\
&\quad + \gamma_a|a_m|^2 + ig_r b_m a_m^* + i(g_l-\xi_m)b_{m-1}a_m^* \\
&\quad - ig_r a_m^* b_m - i(g_l-\xi_{m+1})a_{m+1}^* b_m \\
&\quad + ig_r a_m b_m^* + i(g_l-\xi_{m+1})a_{m+1}b_m^*\Big] \\
&= -\sum_m 2\gamma_a|a_m|^2.
\end{aligned} \tag{A2}$$

Similarly, one can verify that models B, C, and D also respect the norm evolution in Eq. (A1) due to the symmetric couplings.

On the other hand, the RL model could also be extended to include asymmetric couplings. As an example, one could consider a model described by the dynamic equations

$$\begin{aligned}
\frac{\partial a_m}{\partial t} &= -\gamma_a a_m + i(\mu-\chi_{a,m})b_m + i(\nu-\chi_{a,m})b_{m-1}, \\
\frac{\partial b_m}{\partial t} &= i(\mu-\chi_{b,m})a_m + i(\nu-\chi_{b,m})a_{m+1}
\end{aligned} \tag{A3}$$

with $\chi_{\alpha,m} = U|\alpha_m|^2$ ($\alpha = a, b$), which might be viewed as a simple dimerization of the Ablowitz-Ladik equation [40–42]. For such a model, however, the evolution of the norm cannot be simply described by a sum over local decays from each lossy site and the definition of the mean displacement given in Eq. (3) cannot be applied.

Appendix B: Coherent vs incoherent transport

It has been shown that the mean displacement $\langle\Delta m\rangle$ displays continuous dependence on the relative values of ν and μ in the case of incoherent hopping and in the absence of nonlinearities [1]. Moreover, similar incoherent transport behavior has been obtained with on-site nonlinearities due to the interaction-induced decoherence effect [24]. The underlying physics of such results is quite useful for understanding the positive and negative fractional values of $\langle\Delta m\rangle$ in Fig. 2.

For incoherent hopping, the original RL model exhibits continuous variation of $\langle\Delta m\rangle$ from 0 to 1 and thus can also take fractional values. This arises from the competition between the probabilities of the particle hopping from the initial site to all other sites. The particle initially located at site $|m = 0, b\rangle$ can hop to either

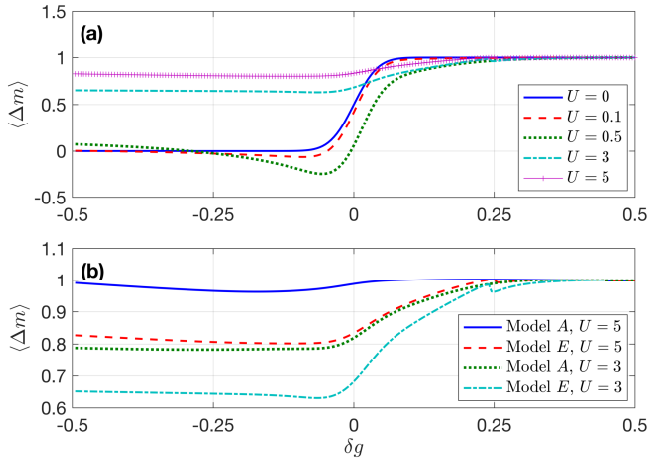

FIG. 7. (Color online) (a) Mean displacement $\langle\Delta m\rangle$ of the particle versus coupling imbalance δg for model E with different values of U. (b) Comparison of $\langle\Delta m\rangle$ versus δg for models A and E with relatively strong nonlinearities. The initial state is assumed as $|\psi(t=0)\rangle = |m=0,b\rangle$. Other parameters are $\mu = 0.5-\delta g$, $\nu = 0.5+\delta g$ and $\gamma_a = 2$.

$|m=0,a\rangle$ or $|m=1,a\rangle$, corresponding to $\langle\Delta m\rangle = 0$ and $\langle\Delta m\rangle = 1$, respectively. However, the contributions of all subsequent hoppings should cancel out in this case (the hopping probabilities from $|m=0,b\rangle$ to $|m=-1,b\rangle$ and to $|m=+1,b\rangle$ are the same). In view of this, the value of $\langle\Delta m\rangle$ is determined by the probability of hopping to A_1 initially, which is given by $\langle\Delta m\rangle = \nu^2/(\nu^2+\mu^2)$ [1, 24].

For models A and B here considered, the fractional values of $\langle\Delta m\rangle$ can be understood in a similar way. However, the most significant difference compared with the linear model above is that the contributions of long-range hopping processes no longer exactly cancel out due to the m-dependent effective couplings, i.e., the effective couplings on the left and right sides of the initial site are no longer symmetric. In particular, also negative fractional values of $\langle\Delta m\rangle$ are allowed, if the left-hand effective couplings are stronger than the right-hand ones.

In Ref. [24], the continuous behavior of $\langle\Delta m\rangle$ is interpreted as the breaking of the translational symmetry of the model arising from the on-site nonlinearity. Such a picture is also applicable to the nonlinear models in this paper which do not respect the translational symmetry due to the position-dependent effective nonlinear couplings.

Appendix C: Nonlinear couplings with only neutral-site contributions

In this appendix, we consider an extended RL model (model E) where the nonlinear intercell couplings only depend on the neutral-site field amplitudes, described by the dynamic equations

$$\begin{aligned} \frac{\partial a_m}{\partial t} &= -\gamma_a a_m + i\mu b_m + i(\nu-\eta_{m-1})b_{m-1}, \\ \frac{\partial b_m}{\partial t} &= i\mu a_m + i(\nu-\eta_m)a_{m+1} \end{aligned} \tag{C1}$$

with $\eta_m = U|b_m|^2$ in this case.

Due to the fact that the particle is initially located at a neutral site with $|\psi(t=0)\rangle = |m=0,b\rangle$, the nearest-neighbor intercell coupling can still be markedly modified at the initial time by the local field amplitude b_0, similar to the case of model A. In view of this, Fig. 7(a) shows qualitatively the same behaviors as those in Fig. 2(a): as U increases, the curve of $\langle\Delta m\rangle$ versus δg tends to be flat, with the values approaching unity over the whole parametric range. In other words, the "trivial-nontrivial" transition in model A can still be achieved even if the nonlinear intercell couplings only depend on the neutral-site field amplitudes. As shown in Fig. 7(b), however, the effective intercell couplings are a bit weaker due to the absence of the contributions of the lossy sites, such that the values of $\langle\Delta m\rangle$ for model E are smaller than those for model A, especially in the region of $\delta g < 0$. To achieve similar modification effects, stronger nonlinearities are required in this case (see for instance the red dashed and green dotted lines).

[1] M. S. Rudner and L. S. Levitov, Topological transition in a non-Hermitian quantum walk, Phys. Rev. Lett. **102**, 065703 (2009).

[2] W. P. Su, J. R. Schrieffer, and A. J. Heeger, Solitons in polyacetylene, Phys. Rev. Lett. **42** 1698-1701 (1979).

[3] M. S. Rudner, M. Levin, and L. S. Levitov, Survival, decay, and topological protection in non-Hermitian quantum transport, arXiv:1605.07652.

[4] J. M. Zeuner, M. C. Rechtsman, Y. Plotnik, Y. Lumer, S. Nolte, M. S. Rudner, M. Segev, and A. Szameit, Observation of a Topological Transition in the Bulk of a Non-Hermitian System, Phys. Rev. Lett. **115**, 040402 (2015).

[5] D. Smirnova, D. Leykam, Y. Chong, and Y. Kivshar, Nonlinear topological photonics, Appl. Phys. Rev. **7**, 021306 (2020).

[6] X. Zhou, Y. Wang, D. Leykam, and Y. D. Chong, Optical isolation with nonlinear topological photonics, New J. Phys. **19**, 095002 (2017).

[7] W. Chen, D. Leykam, Y. Chong, and L. Yang, Nonreciprocity in synthetic photonic materials with nonlinearity, MRS Bull. **43**, 443 (2018).

[8] D. Leykam, S. Mittal, M. Hafezi, and Y. D. Chong, Reconfigurable Topological Phases in Next-Nearest-Neighbor Coupled Resonator Lattices, Phys. Rev. Lett. **121**, 023901 (2018).

[9] A. Amo, When quantum optics meets topology, Science **359**, 638 (2018).

[10] D. A. Dobrykh, A. V. Yulin, A. P. Slobozhanyuk, A. N.

Poddubny, and Y. S. Kivshar, Nonlinear Control of Electromagnetic Topological Edge States, Phys. Rev. Lett. **121**, 163901 (2018).
[11] Y. Hadad, A. B. Khanikaev, and A. Alù, Self-induced topological transitions and edge states supported by nonlinear staggered potentials, Phys. Rev. B **93**, 155112 (2016).
[12] Y. Hadad, J. C. Soric, A. B. Khanikaev, and A. Alù, Self-induced topological protection in nonlinear circuit arrays, Nat. Electronics **1**, 178 (2018).
[13] L. J. Maczewsky, M. Heinrich, M. Kremer, S. K. Ivanov, M. Ehrhardt, F. Martinez, Y. V. Kartashov, V. V. Konotop, L. Torner, D. Bauer, and A. Szameit, Nonlinearity-induced photonic topological insulator, Science **370**, 701 (2020).
[14] M. Ezawa, Nonlinearity-induced transition in the nonlinear Su-Schrieffer-Heeger model and a nonlinear higher-order topological system, Phys. Rev. B **104**, 235420 (2021).
[15] Y. Lumer, M. C. Rechtsman, Y. Plotnik, and M. Segev, Instability of bosonic topological edge states in the presence of interactions, Phys. Rev. A **94**, 021801 (2016).
[16] D. Solnyshkov, O. Bleu, B. Teklu, and G. Malpuech, Chirality of topological gap solitons in bosonic dimer chains, Phys. Rev. Lett. **118**, 023901 (2017).
[17] D. A. Smirnova, L. A. Smirnov, D. Leykam, and Y. S. Kivshar, Topological edge states and gap solitons in the nonlinear Dirac model, Laser Photonics Rev. **13**, 1900223 (2019).
[18] W. Zhang, X. Chen, Y. V. Kartashov, V. V. Konotop, and F. Ye, Coupling of edge states and topological Bragg solitons, Phys. Rev. Lett. **123**, 254103 (2019).
[19] L.-J. Lang, S.-L. Zhu, and Y. D. Chong, Non-Hermitian topological end breathers, Phys. Rev. B **104**, L020303 (2021).
[20] S. Kruk, A. Poddubny, D. Smirnova, L. Wang, A. Slobozhanyuk, A. Shorokhov, I. Kravchenko, B. Luther-Davies, and Y. Kivshar, Nonlinear light generation in topological nanostructures, Nat. Nanotechnol. **14**, 126 (2019).
[21] Y. Wang, L.-J. Lang, C. H. Lee, B. Zhang, and Y. D. Chong, Topologically enhanced harmonic generation in a nonlinear transmission line metamaterial, Nat. Commun. **10**, 1102 (2019).
[22] D. Smirnova, S. Kruk, D. Leykam, E. Melik-Gaykazyan, D.-Y. Choi, and Y. Kivshar, Third-harmonic generation in photonic topological metasurfaces, Phys. Rev. Lett. **123**, 103901 (2019).
[23] S. Xia, D. Kaltsas, D. Song, I. Komis, J. Xu, A. Szameit, H. Buljan, K. G. Makris, Z. Chen, Nonlinear tuning of PT symmetry and non-Hermitian topological states, Science **372**, 72 (2021).
[24] K. Rapedius and H. J. Korsch, Interaction-induced decoherence in non-Hermitian quantum walks of ultracold bosons, Phys. Rev. A **86**, 025601 (2012).
[25] A. K. Harter, A. Saxena, and Y. N. Joglekar, Fragile aspects of topological transition in lossy and parity-time symmetric quantum walks, Sci. Rep. **8**, 12065 (2018).
[26] V. V. Konotop, J. Yang, and D. A. Zezyulin, Nonlinear waves in PT-symmetric systems, Rev. Mod. Phys. **88**, 035002 (2016).
[27] D. Smirnova, D. Leykam, Y. Chong, and Y. Kivshar, Nonlinear topological photonics, Appl. Phys. Rev. **7**, 021306 (2020).
[28] Z.-Y. Xue and Y. Hu, Topological Photonics on Superconducting Quantum Circuits with Parametric Couplings, Adv. Quant. Techn. **4**, 2100017 (2021).
[29] P. Delplace, D. Ullmo, and G. Montambaux, Zak phase and the existence of edge states in graphene, Phys. Rev. B **84**, 195452 (2011).
[30] J. K. Asboth, L. Oroszlany, and A. Palyi, *A short course on topological insulators*, Lecture Notes in Physics, Vol. 919 (Springer International Publishing, Cham, 2016).
[31] L.-H. Li, Z.-H. Xu, and S. Chen, Topological phases of generalized Su-Schrieffer-Heeger models, Phys. Rev. B **89**, 085111 (2014).
[32] S. Lieu, Topological phases in the non-Hermitian Su-Schrieffer-Heeger model, Phys. Rev. B **97**, 045106 (2018).
[33] S. Longhi, Probing one-dimensional topological phases in waveguide lattices with broken chiral symmetry, Opt. Lett. **43**, 4639 (2018).
[34] L. Jin and Z. Song, Bulk-boundary correspondence in a non-Hermitian system in one dimension with chiral inversion symmetry, Phys. Rev. B **99**, 081103(R) (2019).
[35] C. Yuce, Spontaneous topological pumping in non-Hermitian systems, Phys. Rev. A **99**, 032109 (2019).
[36] L. Du, J.-H. Wu, M. Artoni, and G. C. La Rocca, Fractional quantum transport and staggered topological transition in a lossy trimerized lattice, Phys. Rev. A **100**, 052102 (2019).
[37] L. Du, J.-H. Wu, M. Artoni, and G. C. La Rocca, Phase-dependent topological interface state and spatial adiabatic passage in a generalized Su-Schrieffer-Heeger model, Phys. Rev. A **100**, 012112 (2019).
[38] H. C. Wu, L. Jin, and Z. Song, Topology of an anti-parity-time symmetric non-Hermitian Su-Schrieffer-Heeger model, Phys. Rev. B **103**, 235110 (2021).
[39] E. J. Bergholtz, J. C. Budich, and F. K. Kunst, Exceptional topology of non-Hermitian systems, Rev. Mod. Phys. **93**, 015005 (2021).
[40] M. J. Ablowitz and J. F. Ladik, Nonlinear differential–difference equations and Fourier analysis, J. Math. Phys. **17**, 1011 (1976).
[41] M. Salerno, Quantum deformations of the discrete nonlinear Schrödinger equation, Phys. Rev. A **46**, 6856 (1992).
[42] M. Salerno, A new method to solve the quantum Ablowitz-Ladik system, Phys. Lett. A **162**, 381 (1992).
[43] O. Dutta, M. Gajda, P. Hauke, M. Lewenstein, D.-S. Lühmann, B. A Malomed, T. Sowiński, and J. Zakrzewski, Non-standard Hubbard models in optical lattices: a review, Rep. Prog. Phys. **78**, 066001 (2015).
[44] D. Hennig and G. P. Tsironis, Wave transmission in nonlinear lattices, Phys. Rep. **307**, 333 (1999).
[45] S. Lepri and G. Casati, Asymmetric Wave Propagation in Nonlinear Systems, Phys. Rev. Lett. **106**, 164101 (2011).
[46] P. Marquié, J. M. Bilbault, and M. Remoissenet, Observation of nonlinear localized modes in an electrical lattice, Phys. Rev. E **51**, 6127 (1995).